Analytic studies of dispersive properties of shear Alfvén and acoustic wave spectra in tokamaks

Ilija Chavdarovski[1] **and Fulvio Zonca**[1,2]

[1]Institute for Fusion Theory and Simulation, Zhejiang University, Hangzhou 310027, P.R.China

[2]Associazione Euratom-ENEA sulla Fusione, C.R. Frascati, C.P. 65 - 00044 Frascati, Italy

Abstract.

The properties of the low frequency shear Alfvén and acoustic wave spectra in toroidal geometry are examined analytically and numerically considering wave particle interactions with magnetically trapped and circulating particles, using the theoretical model described in *[Chavdarovski I and Zonca F 2009 Plasma Phys. Contr. Fusion* **51** *115001]* and following the framework of the generalized fishbone-like dispersion relation. Effects of trapped particles as well as diamagnetic effects on the frequencies and damping rates of the beta-induced Alfvén eigenmodes (BAE), kinetic balooning Modes (KBM) and beta-induced Alfvén-acoustic eigenmodes (BAAE) are discussed and shown to be crucial to give a proper assessment of mode structure and stability conditions. Present results also demonstrate the mutual coupling of these various branches and suggest that frequency as well as mode polarization are crucial for their identification on the basis of experimental evidence.

PACS numbers: 52.35.Bj, 52.55.Fa, 52.55.Tn

Submitted to: *Plasma Phys. Control. Fusion*

1. Introduction

The low frequency spectrum of Alfvénic fluctuations in tokamak plasmas with $|\omega| \ll \omega_A \equiv v_A/qR_0$, where $v_A = B/\sqrt{4\pi\varrho}$ is the local Alfvén speed, ϱ the plasma mass density, q the safety factor and R_0 the torus major radius, has been subject of intense theoretical and experimental investigation since the discovery of the beta-induced Alfvén eigenmodes (BAE) [3, 4] with frequency below the shear Alfvén continuous spectrum. Experimental evidence exists [5, 6, 7, 8, 9] of modes belonging to both shear Alfvén wave (SAW) and acoustic branches below the "BAE accumulation point" [10] $|\omega| < \omega_{BAE} = \omega_{GAM} \simeq q\omega_{Ti}(7/4 + T_e/T_i)^{1/2}$, where $\omega_{Ti} = v_{Ti}/qR_0$ is the thermal ion transit frequency, v_{Ti} the thermal ion velocity and $T_{i,e}$ the ion and electron temperatures, respectively. Observations in NSTX and JET also show the existence so-called beta induced Alfvén acoustic eigenmodes (BAAE) [11, 12], with generally mixed Alfvén-acoustic polarizations [11, 12, 13, 14, 15, 16] at frequencies $\omega_{BAAE} \sim (T_e/T_i)^{1/2}\omega_{Ti}$. Experimental evidence of BAAE is also reported in DIII-D [17] and HL-2A [18].

At frequencies lower than ω_{BAE}, various physics becomes important, such as coupling of SAW with the slow magneto-acoustic wave (SMW) and resonant wave-particle interaction due to both circulating as well as trapped thermal particles (ions and electrons) in the long mean free path collisionless limit [19]. Because of this, the fluid plasma description can be justified only for modes near the BAE accumulation point and well above the ion transit frequency ($|\omega| \gg \omega_{Ti}$) [10], for which the ion Landau damping becomes negligible. This is achieved for either $q \gg 1$ or $T_e \gg T_i$, which is also the necessary criterion for fluid plasma description of BAAE. In general, it has been shown that validity of the fluid analysis is very limited [10, 20, 1, 21, 22, 23, 24] and kinetic theory is generally needed to deal with the strong wave-particle resonant interactions for BAEs [10, 25, 26, 27, 16, 28, 1], GAMs [29, 30, 31, 32] and BAAEs [23], including diamagnetic effects in the case of BAEs [10, 26, 1, 2] and BAAEs. Kinetic analysis is also necessary when going to even lower frequencies $|\omega| \lesssim \omega_{Bi} \equiv (r/R_0)^{1/2}(T_i/m_i)^{1/2}/(qR_0) \approx \epsilon^{1/2}\omega_{Ti}$, for which trapped thermal ion dynamics becomes crucial [20, 1, 21, 22]. Here, ω_{Bi} is the bounce frequency of deeply trapped ions between magnetic mirror points, r is the radial flux coordinate, and $\epsilon = r/R_0$ is the tokamak local inverse aspect-ratio.

Fluctuations belonging to the low frequency SAW spectrum can be described by one single and general "fishbone-like" dispersion relation in the form [33, 34, 35, 10]

$$i\Lambda(\omega) = \delta\hat{W}_f + \delta\hat{W}_k \quad , \tag{1}$$

which is based on the two scale-length of singular (inertial/kinetic) and regular (ideal MHD) structures of the underlying fluctuations. Here, the left hand side (LHS) is the inertial (kinetic) layer contribution due to thermal particles, while the right hand side (RHS) comes from background MHD and thermal/energetic particle kinetic contributions in the regular ideal regions.

Kinetic layer physics is dominated by thermal ions, while thermal electrons, due to their small mass contribute mainly through trapped electron precessional motion in toroidal direction. Similarly, thermal electrons contribute to $\delta\hat{W}_k$ via resonant as

well as non-resonant responses mostly via their bounce averaged response. Bounce averaged trapped ion dynamics contributes to $\delta\hat{W}_k$ as well and its effect may be of crucial importance in determining the internal kink mode stability in ITER because of ion Landau damping due to the precession resonance ($\omega = \overline{\omega}_{di}$) [36]. Here, $\overline{\omega}_{ds}$ (for $s = e, i$) are the toroidal precessional frequencies for electrons and ions; in particular, $\overline{\omega}_{ds} = \overline{\omega}_{Ds} m_s v^2/2T_s$ for deeply trapped particles, where $\overline{\omega}_{Ds} = (nq/r)T_s/m_s R_0 \omega_{cs}$ and $\omega_{cs} = e_s B/m_s c$. Treating wave-particle resonant interaction and SAW-SMW coupling on the same footing shows that, for $|\omega| \ll \omega_{Bi}$, trapped thermal ion response is not only important, but becomes dominant and $\approx \epsilon^{-1/2}$ larger than that of circulating particles [1]. Hence, it is of crucial importance to include trapped thermal ion dynamics when deriving the dispersion relation of SAW/SMW spectra in toroidal geometry [20, 1, 21, 22].

In this paper we strictly follow Ref. [1], where a simplified model for circulating and trapped particles was applied, considering the former as well circulating with constant parallel velocity along the field lines and the latter as deeply trapped; i.e., characterized by harmonic bounce motion between magnetic mirror points. In a separate and more formal and general work, we will analyze the same problem considered here, in which both circulating and trapped particles are treated in action angle variables, with a realistic description of particle motion in the whole considered frequency range. Here, we describe the structures of low frequency SAW continuous spectrum in low β tokamak plasmas ($\beta = 8\pi P/B_0^2 \approx \epsilon^2$, with P the plasma pressure and B_0 the toroidal magnetic field on axis), taking into account both thermal plasma ion compressibility and diamagnetic effects; thus, $\omega \approx \omega_{*pi} = (T_i c/e_i B^2)(\boldsymbol{k} \times \boldsymbol{B}) \cdot \nabla \ln P_i$, where ω_{*pi} is the thermal plasma ion diamagnetic frequency. SAW/SMW coupling is treated on the same footing of kinetic descriptions of both circulating as well as trapped particles, while finite Larmor radius (FLR) and finite magnetic drift orbit width (FOW) effects are neglected, but can be readily included in the present analysis [26, 25, 37]. For the sake of simplicity, we also assume high poloidal mode numbers with kinetic singular layer at $k_\parallel q R_0 = 0$ [10].

From the expression of Λ given in Ref. [1], it is difficult to visualize the effect of trapped particle dynamics on the low frequency SAW continuous spectrum, due to its complicated mathematical form. For this reason, in this paper we present numerical studies of the previously derived analytic expression of Λ, with the aim of gaining insights into the structures of the low frequency SAW continuous spectrum and of discussing some of its important qualitative features due to trapped particles and diamagnetic effects. In particular, we illustrate properties of frequency and polarization of fluctuations existing in the SAW continuum frequency gaps, particularly BAEs, BAAEs and kinetic balooning modes (KBM). Results discussed in this paper also include kinetic effects on parallel electric field, mode polarization, frequency and damping rates of BAAEs due to the coupling to KBMs. These findings help understanding the actual nature of fluctuations observed experimentally at frequencies well below ω_{BAE}; and suggest that frequency as well as mode polarization are crucial for their identification on the basis of experimental evidence.

This paper is organized as follows. In section 2, we present the theoretical model underlying our kinetic analysis of wave-particle interactions at low frequencies; and summarize the derivation of Λ following strictly Refs. [1, 10] and including both thermal electron and ion responses. Mode polarization properties are also discussed in this section, introducing a frequency dependent complex function that may be used to quantify SAW-SMW coupling and its impact on collisionless damping. Section 3 discusses the fluid limit of Λ and trapped particle as well as diamagnetic effects on the BAE frequency. In section 4, we illustrate the very low frequency limit; and discuss trapped particle and diamagnetic effects on KBM and BAAE modes, as well as effects of their mutual coupling on fluctuation frequency and damping rates. Concluding remarks are given in section 5.

2. Theoretical Model

The generalized fishbone-like dispersion relation (1) is based on the two scale-length asymptotic matching of singular (inertial/kinetic) and regular (ideal MHD) structures of plasma fluctuations. Kinetic layer is characterized by sharply varying radial structure, whose properties are closely related to particle magnetic drifts interaction with perpendicular and parallel electric field [38]. In this paper, we follow the derivation of Λ from Ref. [1], where, for the sake of simplicity in the analysis of the inertial/kinetic layer, all trapped particles are treated as deeply trapped (harmonic $v_\parallel$ between magnetic mirror points) and all circulating particles as well circulating (constant $v_\parallel$). We also employ straight magnetic field line toroidal coordinates (r, ϑ, ζ), with r the radial-like flux coordinate, ϑ the poloidal angle and ζ the generalized toroidal coordinate for which $q = \mathbf{B}\cdot\nabla\zeta/\mathbf{B}\cdot\nabla\vartheta = q(r)$, and the drift frequency can be written as

$$\omega_{dg} = \boldsymbol{k}\cdot\boldsymbol{v}_{dg} = -i\frac{v_\parallel B}{\omega_c}\frac{\partial}{\partial\ell}\left(\frac{\boldsymbol{b}\cdot\boldsymbol{\nabla}r\times\boldsymbol{\nabla}\vartheta}{\boldsymbol{b}\cdot\boldsymbol{\nabla}\vartheta}\frac{v_\parallel}{B}\right)\frac{\partial}{\partial r} \quad , \tag{2}$$

since, in the inertial/kinetic layer, it is dominated by the radial magnetic drifts. Here, $\boldsymbol{v}_{dg}$ is the geodesic particle magnetic drift velocity, $v_\parallel$ the parallel (to $\boldsymbol{B}$) speed, $\omega_c = eB/(mc)$ the cyclotron frequency of a particle of charge e and mass $m, \boldsymbol{b} = \boldsymbol{B}/B\,, \partial/\partial\ell = \boldsymbol{b}\cdot\boldsymbol{\nabla} = (1/B)(\boldsymbol{\nabla}\psi_p\times\boldsymbol{\nabla}\vartheta\cdot\boldsymbol{\nabla}\zeta)\partial/\partial\vartheta$ and $\psi_p = \psi_p(r)$ is the poloidal magnetic flux. The major contribution to perpendicular dynamics is due to ions excursion in the radial direction. Meanwhile, parallel current is dominated by electrons, which have significantly smaller mass than ions and behave as massless fluid that, due to Eq. (2), ensures overall charge neutrality by sustaining a parallel electric field with periodic (a.c.) structure along magnetic field lines [38]. Equation (2) also implies that the flute-like (d.c.) component of the parallel electric field in the long wavelength limit is set by bounce-averaged wave-particle interactions via precessional resonance [1].

The model applied in Ref. [1] assumes a low $\beta \approx \epsilon^2$ axisymmetric tokamak plasma equilibrium with shifted circular flux surfaces, where magnetic shear $s = rq'/q$ and $\alpha = -R_0 q^2\beta'$ define a two-parameter set of plasma equilibria [39] and prime denotes

derivation with respect to r. The plasma state is determined by three fluctuating scalar fields [40, 41]: the scalar potential perturbation $\delta\phi$, the perturbed parallel magnetic field $\delta B_\parallel$ and the perturbed field $\delta\psi$, defined in terms of the parallel vector potential as $\delta A_\parallel = -i(c/\omega)\boldsymbol{b}\cdot\nabla\delta\psi$. With these field variables, the perturbed parallel electric field is given by $\delta E_\parallel = -\boldsymbol{b}\cdot\nabla(\delta\phi - \delta\psi)$ and the ideal magneto-hydrodynamic (MHD) limit is recovered setting $\delta\phi = \delta\psi$, i.e $\delta E_\parallel = 0$. The fluctuating parallel magnetic field, $\delta B_\parallel$, can be explicitly solved for and eliminated form the equations assuming perpendicular pressure balance and substituting $\boldsymbol{\nabla} B$ drift by curvature drift in $\boldsymbol{v_d} = \boldsymbol{b}\times\boldsymbol{\kappa}(\mu B + v_\parallel^2)/\omega_c$ [38, 41], with $\boldsymbol{\kappa} = \boldsymbol{b}\cdot\boldsymbol{\nabla}\boldsymbol{b}$.

The field equations for $\delta\phi$ and $\delta\psi$ are the vorticity equation and quasi-neutrality condition [40, 41]. In the inertial/kinetic layer, such equations are readily written in the "ballooning space", where ϑ is mapped into the extended poloidal angle θ [39]; and, in the long wavelength limit (neglecting finite ion Larmor radius with respect to the radial mode wavelength), vorticity equation and quasi-neutrality condition are given by, respectively [34, 10]

$$B\boldsymbol{b}\cdot\nabla\left[\frac{1}{B}\frac{{k_\perp}^2}{{k_\vartheta}^2}\boldsymbol{b}\cdot\nabla\delta\psi\right] + \frac{\omega^2}{v_A^2}\left(1-\frac{\omega_{*pi}}{\omega}\right)\frac{k_\perp^2}{k_\vartheta^2}\delta\phi + \frac{\alpha}{q^2R^2}g(\theta)\delta\psi = \left\langle\frac{4\pi e}{k_\vartheta^2c^2}\omega\omega_{di}\delta K_i\right\rangle, \tag{3}$$

$$\left(1+\frac{1}{\tau}\right)(\delta\phi-\delta\psi) = \frac{T_i}{ne}\langle\delta K_i - \delta K_e\rangle, \tag{4}$$

where $\langle(...)\rangle = \int d\boldsymbol{v}(...)$ denotes integration in velocity space, $\boldsymbol{b}\cdot\nabla = (qR_0)^{-1}\partial_\theta$, R_0 is the tokamak major radius, $k_\perp^2/k_\vartheta^2 = 1 + k_r^2/k_\vartheta^2 = 1 + (s\theta - \alpha\sin\theta)^2$, k_r and k_ϑ are radial and poloidal wave vectors, respectively, and $g(\theta) = \cos\theta + [s\theta - \alpha\sin\theta]\sin\theta$. Furthermore, for each particle species $s = e, i$, $\omega_{*ps} = \omega_{*ns} + \omega_{*Ts}$, $\omega_{*ns} = (T_sc/e_sB)(\boldsymbol{k}\times\boldsymbol{b})\cdot\nabla(n_s)/n_s, \omega_{*Ts} = (T_sc/e_sB)(\boldsymbol{k}\times\boldsymbol{b})\cdot\nabla(T_s)/T_s$, n_s is the particle density, $\tau = T_e/T_i$, $n_e = n_i = n$ and we assume only one thermal ion species with unit electric charge.

In the kinetic layer, the fields have a sharply varying radial structure with $k_\perp^2/k_\vartheta^2 \gg 1$ or, equivalently, $s^2|\theta|^2 \gg 1$. For the optimal frequency ordering $|k_\parallel|v_A \approx \omega_{Ti} = (2T_i/m_i)^{1/2}/(qR_0)$ and $|s| = O(1)$, v_A being the Alfvén speed, one readily obtains $|\theta| = O(\beta^{-1/2})$ in the kinetic layer since $|k_\parallel|qR_0 \approx |\theta|^{-1} \approx \beta^{1/2}$ [10], with $k_\parallel$ the parallel (to $\boldsymbol{b}$) wave vector. For large $|\theta| = O(\beta^{-1/2})$, the fluctuating fields show a two scale behavior: they vary on a short scale $\theta_0 \approx 1$ and on a long scale $\theta_1 \approx O(\beta^{-1/2})$. Although this ordering is strictly derived for circulating particles, it can be readily extended to include magnetically trapped particles, for which $|\theta_0/\theta_1| \ll 1$ still applies [1]. For convenience [38], it is useful to adopt the rescaled fluctuating potentials $\delta\Phi = (k_\perp/k_\vartheta)\delta\phi$ and $\delta\Psi = (k_\perp/k_\vartheta)\delta\psi$, and represent them as asymptotic series in powers of $\beta^{1/2}$; e.g., $\delta\Phi = \delta\Phi^{(0)} + \delta\Phi^{(1)} + \delta\Phi^{(2)} + ...$, where $\delta\Phi^{(1)} = O(\beta^{1/2})$, $\delta\Phi^{(2)} = O(\beta)$, etc.

Following Refs. [1] and [10], we easily show that $\delta\Psi^{(0)} = \delta\Psi^{(0)}(\theta_1)$ and $\delta\Psi^{(1)} = 0$, while, on the other hand, $\delta\Phi \simeq \delta\Phi^{(0)}(\theta_1) + \delta\Phi_s(\theta_1)\sin\theta_0$ up to order $\beta^{1/2}$, where $\delta\Phi_s(\theta_1)$, $\delta\Phi^{(0)}(\theta_1)$ and $\delta\Psi^{(0)}(\theta_1)$ vary only on the long scale θ_1. One generally has

$\delta\Phi^{(0)}(\theta_1) \sim \delta\Psi^{(0)}(\theta_1)$, while $\delta\Phi_s(\theta_1) \sim \delta\Phi^{(0)}(\theta_1)$ for $\omega \sim \overline{\omega}_{Di} = k_\vartheta(cT_i)/(eBR_0)$ (the precessional frequency) and $\delta\Phi_s(\theta_1) \sim O(\beta^{1/2})\delta\Phi^{(0)}(\theta_1)$ for $\omega \sim \omega_{Ti}$ [1, 23].

Solving for the kinetic responses of thermal electrons and ions in the layer region, it is possible to show [1]

$$\delta\Phi^{(0)} = I_\Phi(\omega/\overline{\omega}_{Di}, \omega/\overline{\omega}_{De})\delta\Psi^{(0)} \quad , \tag{5}$$

with $\overline{\omega}_{De} = -\tau\overline{\omega}_{Di}$ and

$$I_\Phi\left(\frac{\omega}{\overline{\omega}_{Di}}, \frac{\omega}{\overline{\omega}_{De}}\right) = 1 + \frac{\sqrt{2\epsilon}\tau\left(L(\omega/\overline{\omega}_{Di}) + \tau^{-1}L(\omega/\overline{\omega}_{De})\right)}{1 + \tau\omega_{*ni}/\omega + \sqrt{2\epsilon}\tau\left[1 - \omega_{*ni}/\omega - M(\omega/\overline{\omega}_{Di}) - \tau^{-1}M(\omega/\overline{\omega}_{De})\right]} \quad . \tag{6}$$

Here, $\epsilon = r/R_0$,

$$\begin{aligned} M\left(\frac{\omega}{\overline{\omega}_{Di}}\right) = & -2\frac{\omega}{\overline{\omega}_{Di}}\left\{\left(1 - \frac{\omega_{*ni}}{\omega} + \frac{3}{2}\frac{\omega_{*Ti}}{\omega}\right)\left[1 + \sqrt{\frac{\omega}{\overline{\omega}_{Di}}}Z\left(\sqrt{\frac{\omega}{\overline{\omega}_{Di}}}\right)\right]\right. \\ & \left. - \frac{\omega_{*Ti}}{\omega}\left[\frac{1}{2} + \frac{\omega}{\overline{\omega}_{Di}} + \left(\frac{\omega}{\overline{\omega}_{Di}}\right)^{3/2} Z\left(\sqrt{\frac{\omega}{\overline{\omega}_{Di}}}\right)\right]\right\} \end{aligned} \tag{7}$$

and

$$\begin{aligned} L\left(\frac{\omega}{\overline{\omega}_{Di}}\right) = & -2\left\{\left(1 - \frac{\omega_{*ni}}{\omega} + \frac{3}{2}\frac{\omega_{*Ti}}{\omega}\right)\left[\frac{1}{2} + \frac{\omega}{\overline{\omega}_{Di}} + \left(\frac{\omega}{\overline{\omega}_{Di}}\right)^{3/2} Z\left(\sqrt{\frac{\omega}{\overline{\omega}_{Di}}}\right)\right]\right. \\ & \left. - \frac{\omega_{*Ti}}{\omega}\left[\frac{3}{4} + \frac{1}{2}\frac{\omega}{\overline{\omega}_{Di}} + \left(\frac{\omega}{\overline{\omega}_{Di}}\right)^{2} + \left(\frac{\omega}{\overline{\omega}_{Di}}\right)^{5/2} Z\left(\sqrt{\frac{\omega}{\overline{\omega}_{Di}}}\right)\right]\right\} \quad , \end{aligned} \tag{8}$$

with $Z(x) = 1/\sqrt{\pi}\int_{-\infty}^{\infty} e^{-y^2}/(y - x)\, dy$. The corresponding functions for trapped electrons $M(\omega/\overline{\omega}_{De})$ and $L(\omega/\overline{\omega}_{De})$ are obtained from Eqs. (7) and (8) by substitution $\overline{\omega}_{Di}, \omega_{*ni}, \omega_{*Ti} \rightarrow \overline{\omega}_{De}, \omega_{*ne}, \omega_{*Te}$. Equation (5) shows that the d.c. component of the parallel electric field, $\propto \delta\Phi^{(0)} - \delta\Psi^{(0)}$, is connected with the existence of trapped particles and the precessional resonance, since $I_\Phi \rightarrow 1$ for $\epsilon \rightarrow 0$. Furthermore, for $|\omega| \gg |\overline{\omega}_{Di,e}|, |\omega_{*pi,e}|$, one can show $M\left(\omega/\overline{\omega}_{Di}\right) \rightarrow (1 - \omega_{*ni}/\omega)$ and $L\left(\omega/\overline{\omega}_{Di}\right) \rightarrow \overline{\omega}_{Di}/\omega$; thus, again, reducing Eq. (6) to $I_\Phi = 1$.

The existence of finite d.c. parallel electric field is due to $I_\phi \neq 1$ and, in the long wavelength limit, it is due to the resonant wave-plasma interaction at trapped particle precession frequency. In Fig. 1 we show real and imaginary parts of I_ϕ for different frequencies, assuming $\overline{\omega}_{De} = -\overline{\omega}_{Di}$ and $-\omega_{*e} = \omega_{*i} = 0.2\omega_{Ti}$. The figure shows that I_ϕ is generally not equal to 1, but for a large portion of the spectrum, *i.e.*, when $\omega > \omega_{Ti}$, the simplified expressions $\mathbb{R}\mathrm{e}I_\Phi \simeq 1$ and $\mathbb{I}\mathrm{m}I_\Phi \simeq 0$ are reasonably good approximations. In fact, for the parameters given in Fig. 1, around the frequency of BAE accumulation point $I_\Phi \approx 0.989$. For the same parameters we also have $I_\phi = 1$ when $\omega \rightarrow 0$. However, we, again, remind the reader that, in order to make a general statement about the value of I_ϕ a treatment is required that includes correct particle motion and finite Larmor radius effects. In the present approximative model, it is evident that the appearance of finite d.c. parallel electric field is due to particle precessional resonance with both thermal electrons and ions, $\omega \simeq \overline{\omega}_{De,i}$ accounted for by the plasma dispersion functions

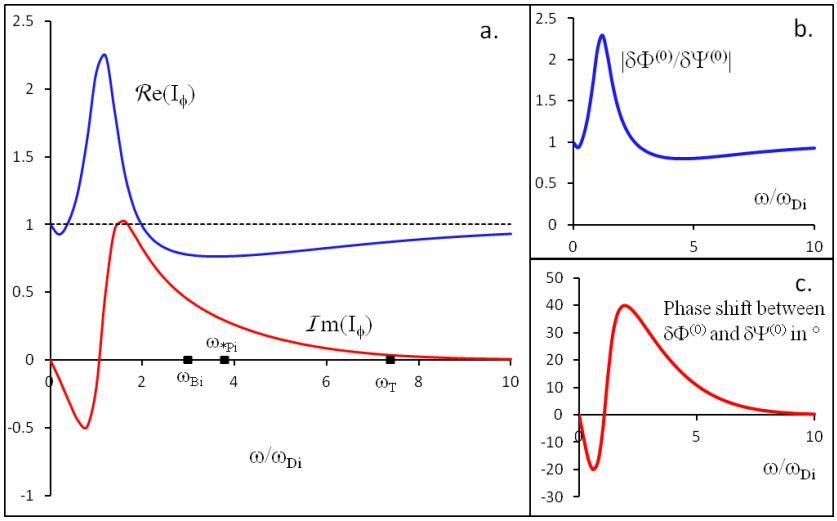

Figure 1. a.Values of $\mathbb{R}\mathrm{e}I_\Phi$ (upper line) and $\mathbb{I}\mathrm{m}I_\Phi$ (bottom line) as functions of $\mathbb{R}\mathrm{e}(\omega/\bar{\omega}_{Di})$ for fixed parameters $\omega_{*ni}/\omega_{Ti} = \omega_{*Ti}/\omega_{Ti} = 0.2$, $\bar{\omega}_{Di}/\omega_{Ti} = 0.15/\sqrt{2}$, $q = 1.5$ and $\tau = 1$; b. The ratio $\mid \delta\Phi^{(0)}/\delta\Psi^{(0)} \mid$ and c. The phase shift between $\delta\Phi^{(0)}$ and $\delta\Psi^{(0)}$ for the same parameters.

in Eq. (6). This can be understood, since electrons and ions have $\overline{\omega}_{De} = -\tau\overline{\omega}_{Di}$. In this way, electrons are not able to short circuit the d.c. parallel electric field if $|\omega| \sim |\overline{\omega}_{De,i}|$.

The expression of I_ϕ is a function of precessional and diamagnetic frequencies of thermal ions and electrons. Hence, in general, we can speak of precessional and diamagnetic effects on the d.c. parallel electric field. Since d.c. parallel electric field also exists due to the finite Larmor radius (FLR) effects [42, 43], for a complete the picture one needs to consider both thermal ion FLR effects as well as precessional resonance of both ions and electrons on the same footing.It is worthwhile noting that I_ϕ has a significant imaginary part (lower line of Fig. 1a), which in real space corresponds to a phase shift between the perturbed $\delta\Phi$ and $\delta\Psi$ (see Fig. 1c), which is not case when only FLR are considered. These effects will be studied and discussed in a separate work.

Further solving the quasineutrality condition for the sinusoidal term in the inertial region we obtain [1]:

$$\delta\Phi_s = -\frac{N_1(\frac{\omega}{\omega_{Ti}}) + \Delta N_1(\frac{\omega}{\omega_{Ti}}) + \sqrt{2\epsilon}P_2(\frac{\omega}{\overline{\omega}_{Di}}, \frac{\omega_{Bi}}{\overline{\omega}_{Di}})}{1 + \frac{1}{\tau} + D_1(\frac{\omega}{\omega_{Ti}}) + \Delta D_1(\frac{\omega}{\omega_{Ti}}) + \sqrt{2\epsilon}\left[P_1(\frac{\omega}{\overline{\omega}_{Di}}, \frac{\omega_{Bi}}{\overline{\omega}_{Di}}) - P_2(\frac{\omega}{\overline{\omega}_{Di}}, \frac{\omega_{Bi}}{\overline{\omega}_{Di}})\right]}\xi\delta\Phi^{(0)}\,, \quad (9)$$

where $P_1(\omega/\overline{\omega}_{Di}, \omega_{Bi}/\overline{\omega}_{Di})$ and $P_2(\omega/\overline{\omega}_{Di}, \omega_{Bi}/\overline{\omega}_{Di})$ come from the trapped particles dynamics and can be calculated as:

$$P_1(\omega/\overline{\omega}_{Di}, \omega_{Bi}/\overline{\omega}_{Di}) = -2\frac{\omega^2}{\overline{\omega}_{Di}^2}\left[(1 - \frac{\omega_{*n}}{\omega} + \frac{3}{2}\frac{\omega_{*T}}{\omega})G_2 - \frac{\omega_{*T}}{\omega}G_4\right]\,,$$

$$P_2(\omega/\overline{\omega}_{Di}, \omega_{Bi}/\overline{\omega}_{Di}) = -2\frac{\omega}{\overline{\omega}_{Di}}\left[(1 - \frac{\omega_{*n}}{\omega} + \frac{3}{2}\frac{\omega_{*T}}{\omega})G_4 - \frac{\omega_{*T}}{\omega}G_6\right]\,;$$

and we have denoted

$$G_n = \frac{1}{\pi^{1/2}} \int_{-\infty}^{\infty} \frac{e^{-x^2} x^n}{(\omega/\overline{\omega}_{Di} - x^2)^2 - (\omega_{Bi}/\overline{\omega}_{Di})^2 x^2}\, dx\,,$$

for $n = 2, 4, 6, 8$. Following Ref.[1], we adopt the definition $\delta\Phi_s = S(\omega, \overline{\omega}_{Di}, \omega_{Bi}, \omega_{Ti})\xi\delta\Phi^{(0)}$ to indicate the relation in Eq. (9), while the G_n integrals become [1]

$$G_2 = \frac{\overline{\omega}_{Di}/\omega_{Bi}}{\Omega_1 + \Omega_2}\left[\Omega_1 Z(\Omega_1) - \Omega_2 Z(\Omega_2)\right] \ ,$$

$$G_4 = \frac{\overline{\omega}_{Di}/\omega_{Bi}}{\Omega_1 + \Omega_2}\left[\Omega_1^2 - \Omega_2^2 + \Omega_1^3 Z(\Omega_1) - \Omega_2^3 Z(\Omega_2)\right] \ ,$$

$$G_6 = \frac{\overline{\omega}_{Di}/\omega_{Bi}}{\Omega_1 + \Omega_2}\left[(1/2)(\Omega_1^2 - \Omega_2^2) + \Omega_1^4 - \Omega_2^4 + \Omega_1^5 Z(\Omega_1) - \Omega_2^5 Z(\Omega_2)\right] \ ,$$

$$G_8 = \frac{\overline{\omega}_{Di}/\omega_{Bi}}{\Omega_1 + \Omega_2}\left[(3/4)(\Omega_1^2 - \Omega_2^2) + (1/2)(\Omega_1^4 - \Omega_2^4) + \Omega_1^6 - \Omega_2^6 + \Omega_1^7 Z(\Omega_1) - \Omega_2^7 Z(\Omega_2)\right] \ ,$$

with Ω_1 and Ω_2 defined as

$$\Omega_1 = \frac{\frac{\omega_{Bi}}{\overline{\omega}_{Di}} + \sqrt{(\frac{\omega_{Bi}}{\overline{\omega}_{Di}})^2 + 4\frac{\omega}{\overline{\omega}_{Di}}}}{2} \text{ and } \Omega_2 = \frac{-\frac{\omega_{Bi}}{\overline{\omega}_{Di}} + \sqrt{(\frac{\omega_{Bi}}{\overline{\omega}_{Di}})^2 + 4\frac{\omega}{\overline{\omega}_{Di}}}}{2} \ .$$

Furthermore, in Eq. (9), the functions

$$D_1(x) = x\left(1 - \frac{\omega_{*ni}}{\omega}\right) Z(x) - \frac{\omega_{*Ti}}{\omega} x[x + (x^2 - 1/2)Z(x)] \tag{10}$$

and

$$N_1(x) = 2(\overline{\omega}_{Di}/\omega_{Ti})N(x) \ ,$$

with

$$N(x) = \left(1 - \frac{\omega_{*ni}}{\omega}\right)[x + (1/2 + x^2)Z(x)] - \frac{\omega_{*Ti}}{\omega}[x(1/2 + x^2) + (1/4 + x^4)Z(x)] \ , \tag{11}$$

come from the well circulating particles dynamics [10], whereas the functions $\Delta N_1(x)$ and $\Delta D_1(x)$ account for circulating particle dynamic modification due to finite trapped particle fraction [1]:

$$\Delta D_1(x) = \frac{x}{\pi^{1/2}} \int_0^{\infty} e^{-y} \ln\left(\frac{x + \sqrt{2\epsilon y}}{x - \sqrt{2\epsilon y}}\right)\left[1 - \frac{\omega_{*ni}}{\omega} - \frac{\omega_{*Ti}}{\omega}\left(y - \frac{3}{2}\right)\right] dy \ , \tag{12}$$

$$\Delta N_1(x) = \frac{\overline{\omega}_{Di}/\omega_{Ti}}{\pi^{1/2}} \int_0^{\infty} y e^{-y} \ln\left(\frac{x + \sqrt{2\epsilon y}}{x - \sqrt{2\epsilon y}}\right)\left[1 - \frac{\omega_{*ni}}{\omega} - \frac{\omega_{*Ti}}{\omega}\left(y - \frac{3}{2}\right)\right] dy \ . \tag{13}$$

Here, the logarithmic term in the integrands is numerically calculated as $\ln(x + \sqrt{2\epsilon y}) - \ln(x - \sqrt{2\epsilon y})$ for ensuring proper analytic continuation [1].

Following Ref. [10, 1], the vorticity equation at second order in the asymptotic expansion is reduced to the form $(\partial^2/\partial\theta_1^2)\delta\Psi^{(0)} + \Lambda^2\delta\Psi^{(0)} = 0$, where the general expression of Λ^2 can be written as:

$$\Lambda^2/I_\Phi = \frac{\omega^2}{\omega_A^2}\left(1 - \frac{\omega_{*pi}}{\omega}\right) + \Lambda_{cir}^2 + \Lambda_{tra}^2 \ , \tag{14}$$

where Λ^2_{cir} and Λ^2_{tra} are the circulating and trapped particles contributions with

$$\Lambda^2_{tra} = \frac{\omega^2\omega^2_{Bi}}{\omega^2_A\overline{\omega}^2_{Di}}\frac{q^2}{\sqrt{2\epsilon}}\left[P_3 + (P_2 - P_3)S(\omega, \overline{\omega}_{Di}, \omega_{Bi}, \omega_{Ti})\right] \tag{15}$$

and

$$P_3 = -2\left[(1 - \frac{\omega_{*n}}{\omega} + \frac{3}{2}\frac{\omega_{*T}}{\omega})G_6 - \frac{\omega_{*T}}{\omega}G_8\right] \ .$$

The circulating particle term [10] contains the well circulating response and corrections due to trapped particle fraction

$$\Lambda^2_{cir} = q^2\frac{\omega\omega_{Ti}}{\omega^2_A}\left[\left(1 - \frac{\omega_{*ni}}{\omega}\right)\left(F\left(\frac{\omega}{\omega_{Ti}}\right) + \Delta F\left(\frac{\omega}{\omega_{Ti}}\right)\right) - \frac{\omega_{*Ti}}{\omega}\left(G\left(\frac{\omega}{\omega_{Ti}}\right)\right.\right.$$
$$\left.\left. + \Delta G\left(\frac{\omega}{\omega_{Ti}}\right)\right) + \frac{\omega\omega_{Ti}}{4\overline{\omega}^2_{Di}}\left(N_1\left(\frac{\omega}{\omega_{Ti}}\right) + \Delta N_1\left(\frac{\omega}{\omega_{Ti}}\right)\right)S(\omega, \overline{\omega}_{Di}, \omega_{Bi}, \omega_{Ti})\right] \ ,$$

which reduces to the well circulating particle response given by [10] in the $\epsilon \to 0$ limit. The functions within the brackets are [10]:

$$F(x) = x\left(x^2 + 3/2\right) + \left(x^4 + x^2 + 1/2\right)Z(x) \, ,$$
$$G(x) = x\left(x^4 + x^2 + 2\right) + \left(x^6 + x^4/2 + x^2 + 3/4\right)Z(x) \, , \tag{16}$$

and $\Delta F(\omega/\omega_{Ti})$ and $\Delta G(\omega/\omega_{Ti})$ are given by [1]:

$$\Delta F(x) = \frac{1}{\pi^{1/2}}\int_0^\infty e^{-y}\ln\left(\frac{x + \sqrt{2\epsilon y}}{x - \sqrt{2\epsilon y}}\right)\frac{y^2}{4}dy \ \ , \tag{17}$$

$$\Delta G(x) = \frac{1}{\pi^{1/2}}\int_0^\infty e^{-y}\ln\left(\frac{x + \sqrt{2\epsilon y}}{x - \sqrt{2\epsilon y}}\right)\frac{y^2}{4}\left(y - \frac{3}{2}\right)dy. \tag{18}$$

The final term of Λ in Eq. (14) contains transit frequency resonance at $\omega = \omega_{Ti}$ and combined bounce/precession resonance $\omega = \overline{\omega}_{Di} \pm \omega_{Bi}$. In fact, as noted above the precessional resonance $\omega = \overline{\omega}_{Di,e}$ in the kinetic layer only contributes to the d.c. parallel electric field term $\propto I_\Phi$ defined in Eq. (6). Thus, besides the $\tau = T_e/T_i$ factor in the quasi-neutrality equation, the $\propto I_\Phi$ term is the only way electron dynamics affects the kinetic layer, assuming negligible inertia. Note that Eq. (14), similarly to Eq. (6), is valid up to $\mathrm{O}(\epsilon^{1/2})$ with respect to the leading order; and that higher order terms must be neglected for consistency in the present asymptotic expansion.

The expression for Λ in Eq. (14) may be used in the general fishbone-like dispersion relation, Eq. (1), for describing a variety of shear Alfvén modes in a wide frequency range, from 0 to ω_{BAE}. Note, however, that potentially important effects, such as precession reversal and the contribution of barely trapped/circulating particles are not included in Eq. (14). The accumulation points of the shear Alfvén continuous spectrum are simply found by solving $\Lambda = 0$ with the complex frequency ω as root. The complex accumulation point frequency is indicative of the corresponding type of fluctuation that may be reasonably expected, since all modes "emerge" from the accumulation points for increasing values of $\delta\hat{W}_f$ and/or $\delta\hat{W}_k$, as it is readily recognized from Eq. (1) [44]. Specific examples are discussed below in sections 3 and 4.

3. Fluid limit of Λ and BAE spectrum

Extensive studies of the effects of circulating ions on the BAE spectrum [10, 26, 27, 23] enable us to elucidate the trapped particle influence on the high frequency spectrum by observing the changes to the previous results when a trapped ion population is introduced. In the high frequency limit, $|\omega| \gg \omega_{Ti}$, it was shown that the circulating particle contribution reduces to [1, 10]

$$\Lambda^2_{cir} = -\frac{\omega^2}{\omega_A^2} q^2 \frac{\omega_{Ti}^2}{\omega^2} \left[\left(\frac{7}{4} + \tau \right) - \frac{3}{4}\sqrt{2\epsilon} \left(\frac{5}{4} + \tau \right) \right] , \tag{19}$$

where, for simplicity, the $\omega_{*pi}/\omega \to 0$ limit is considered. The first term in the brackets comes from $F(x)$ and accounts for well circulating particles [10], while the $\propto \sqrt{2\epsilon}$ contribution comes from ΔF and describes the modified circulating particle response only, since the $S(\omega, \overline{\omega}_{Di}, \omega_{Bi}, \omega_{Ti})$ function becomes independent of $\sqrt{2\epsilon}$ at high frequency [1].

For the trapped particle term, we expand the final result in $\omega_{Bi}/\omega \to 0$ and get:

$$\Lambda^2_{tra} = -\frac{3}{4}\sqrt{2\epsilon} \frac{\omega^2}{\omega_A^2} q^2 \frac{\omega_{Ti}^2}{\omega^2} \left(\frac{5}{4} + \tau \right) , \tag{20}$$

As stated above, the trapped particles effect is of order $\sqrt{2\epsilon}$ with respect to that of circulating particles and cancels the $\propto \sqrt{2\epsilon}$ terms in the circulating particle response at high frequency. The combination of Eqs. (19) and (20) into Eq. (14) gives accumulation points at $\Lambda = 0$; *i.e.*,

$$\omega_{BAE} = \pm q \omega_{Ti} \sqrt{\left(\frac{7}{4} + \tau \right)} , \tag{21}$$

which is the same result for the BAE accumulation point frequency as when only well circulating particles are taken into account [10]. Both Eq. (21) and previous analytical results [1, 2] indicate that BAE accumulation point frequency is not affected by the presence of trapped particles at the lowest order in the trapped particle fraction expansion. This means that trapped ion effects cancel out barely circulating ion response up to order ϵ. In other words, in this frequency limit we can treat the thermal plasma as if it were composed of well circulating particles only. However, this assumption is only valid for the approximate model adopted here, treating particles as either deeply trapped or well circulating. When a proper treatment is used for the entire particle population, barely trapped and barely circulating particles included, an order $O(\epsilon^{1/2})$ frequency shift is expected to appear, as it is argued in the following.

The cancelation of barely circulating and deeply trapped particle contributions can be verified in Fig. 2, where the real ($\mathbb{R}\mathrm{e}\Lambda^2$) and imaginary part ($\mathbb{I}\mathrm{m}\Lambda^2$) of Λ are plotted against the real part of the frequency ω normalized to ω_{Ti}, for the cases with only circulating particles (presented with full circles for real and empty circles for imaginary) and the case when trapped particles are included (full and empty squares, analogously). In all cases in this paper, unless otherwise specified, we will take $q = 1.5$, $\tau = 1$ and $v_{Ti}^2/v_A^2 = 0.01$. In a previous work [1], a numerical calculation of the analytic dispersion

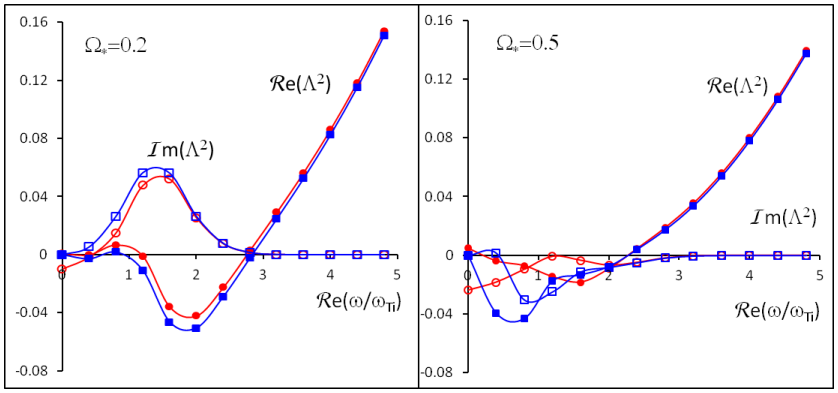

Figure 2. Values of $\mathbb{R}\mathrm{e}\Lambda^2$ ($\epsilon = 0$ full circles; $\epsilon = 0.1$ full squares) and $\mathbb{I}\mathrm{m}\Lambda^2$ ($\epsilon = 0$ open circles; $\epsilon = 0.1$ open squares) are shown vs. $\mathbb{R}\mathrm{e}(\omega/\omega_{Ti})$ for fixed parameters $\bar{\omega}_{Di}/\omega_{Ti} = 0.15/\sqrt{2}$, $q = 1.5$, $\tau = 1$, $\eta_i = \omega_{*Ti}/\omega_{*ni} = 1$ and a. $\Omega_* = \omega_{*ni}/\omega_{Ti} = 0.2$ and b. $\Omega_* = 0.5$.

relation was presented, based on an inaccurate complex root finding routine, the result of which was a significant shift of the curves in the high frequency regime (see Fig.1 of that paper). The improved numerical assessment, shown here, corrects that inaccuracy and demonstrates the cancelation of trapped and circulating particle responses up to order ϵ, as predicted by Eqs. (19) and (20). In Fig. 2, the values of Λ are almost identical with and without trapped particles as implied by Eq. (21) and Ref [1, 2] for large frequencies ($\omega \gg \omega_{Ti}$); and, hence, the BAE accumulation point $\Lambda = 0$ is not affected by the trapped particle population. This conclusion is also valid for GAM, due to the degeneracy of BAE and GAM spectra in the long wavelength limit ($\Lambda = 0$ and $\omega_{*pi} = 0$) [38, 45, 44, 46, 47].

The difference in the shear Alfvén continuous spectrum, due to trapped particles, becomes significant at low frequency ($\omega \ll \omega_{BAE}$), as it is shown in Fig. 2. This difference becomes even more evident with stronger diamagnetic effects (see Fig. 2b), when the same plots are made for $\Omega_* = \omega_{*ni}/\omega_{Ti} = 0.5$ instead of $\Omega_{*ni} = 0.2$. We note, again, that the plots are almost identical at high frequency, but the behavior at low frequency is significantly affected by the precession-bounce resonance with trapped thermal ions. In Fig. 2b, it is evident that at the high frequency accumulation point, where $\mathbb{R}\mathrm{e}\Lambda^2$ crosses zero with positive slope and negative $\mathbb{I}\mathrm{m}\Lambda^2$, the accumulation point itself has a positive imaginary part, as noted in [10], due to finite thermal gradient effects coming from $\eta_i = \omega_{*Ti}/\omega_{*ni} = 1$. The existence of an unstable accumulation point in the shear Alfvén continuous spectrum is not an issue as, in one e-folding time, the corresponding fluctuating field develops fine scale lengths, where finite ion Larmor radius and finite magnetic orbit width play important role [10]. Then, either the continuous spectrum is discretized and the short wavelength mode becomes a kinetic BAE [26, 48], or a discrete Alfvénic ion temperature gradient driven mode (AITG) is formed in the BAE frequency gap in the shear Alfvén continuum [27, 38, 44], provided that $\delta\hat{W}_f + \mathbb{R}e\delta\hat{W}_k < 0$ in the general "fishbone-like" dispersion relation, Eq. 1. The

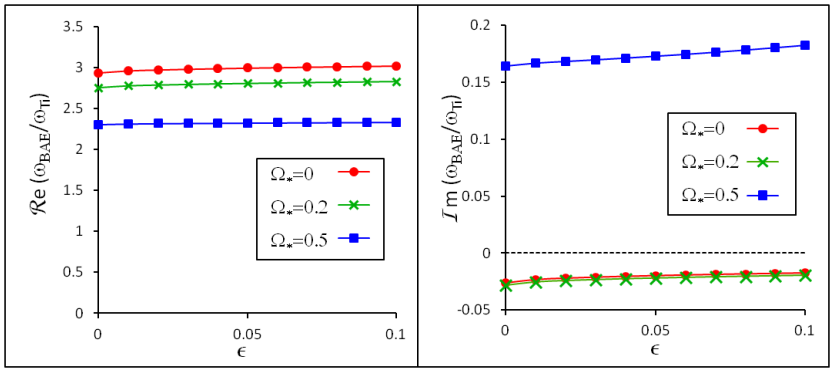

Figure 3. a.The real part of accumulation frequency of BAE spectrum shown vs. ϵ for three values of $\Omega_* = \omega_{*ni}/\omega_{Ti} = \omega_{*Ti}/\omega_{Ti} = 0$, 0.2 and 0.5 and fixed parameters $\bar{\omega}_{Di}/\omega_{Ti} = 0.15/\sqrt{2}$, $q = 1.5$, $\tau = 1$; b.The imaginary part of the of accumulation frequency of BAE for the same parameters.

lower frequency counterpart of AITG is the kinetic ballooning mode (KBM) branch modified by wave-particle resonances, for which trapped particle effects are crucially important, as shown in Fig. 2b. For sufficiently short wavelength, such that the thermal ion diamagnetic drift is much larger than the thermal ion transit frequency ($|\omega_{*pi}| \gg \omega_{Ti}$), this branch connects to the usual KBM branch [49], discussed in the literature since the early 1980s.

In Fig. 3 the accumulation point of the BAE spectrum is shown against ϵ, *i.e.*, against increasing trapped ion population, for different values of Ω_*. In all cases, the BAE frequency is un-affected by the change of ϵ, in agreement with Eq. (21). On the other hand, numerical simulation results by the LIGKA code [21, 22] used for analyzing BAE excited by ICRH energetic ions tails in AUG, show significant lowering of the BAE frequency due to trapped particle population. Thus, we reasonably deduce that this $O(\epsilon^{1/2})$ frequency shift is predominantly due to barely trapped/circulating particle population. Meanwhile, the fact that barely trapped particle dynamics may be significantly affected by collisions, depending on the collisionality regime, suggests that the trapped particle induced $O(\epsilon^{1/2})$ shift of the BAE frequency should depend on plasma collisionality, and, hence, that BAE/GAM frequency shift should depend on plasma density. This issue will be dealt with in a more detailed study of the BAE/GAM frequency spectrum using action-angle formulation for the analysis of general particle motions.

The fact that the $O(\epsilon^{1/2})$ shift is not coming from the diamagnetic effects can be seen from Fig. 4, where the real and imaginary parts of BAE accumulation point are given against Ω_* for two different values of $\eta_i = 0$ and 1. The lines with squares represent the expressions with trapped particles included ($\epsilon = 0.1$), the full line with circulating particles only ($\epsilon = 0$), while the dashed line shows $\omega_{*pi} = \omega_{*ni} + \omega_{*Ti}$. The line with crosses, shows existence of another solution to the BAE dispersion relation, which typically has a large negative imaginary part as in the case of many further solutions to the dispersion relation due to the transcendental nature of the Z function.

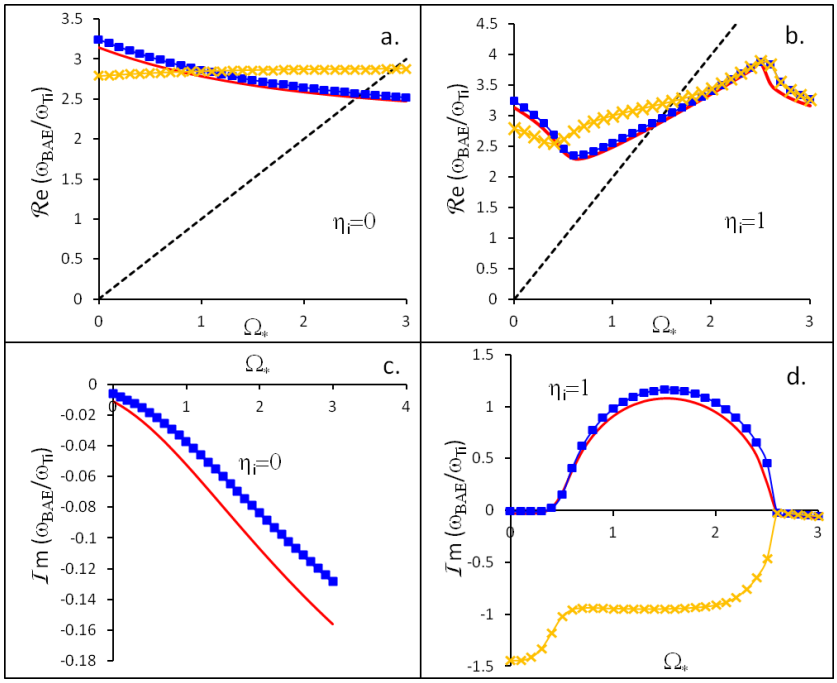

Figure 4. The real and imaginary part of accumulation frequency of BAE spectrum shown vs. $\Omega_* = \omega_{*ni}/\omega_{Ti}$ for fixed parameters $\bar{\omega}_{Di}/\omega_{Ti} = 0.15/\sqrt{2}$, $q = 1.5$, $\tau = 1.5$; with $\eta_i = 0$ (Figures a and c), and $\eta_i = 1$ (Figures b and d). Circulating particles only $\epsilon = 0$ (full line), trapped ions included $\epsilon = 0.1$ (presented with squares). The dashed line is ω_{*pi}/ω_{Ti}, and the line with crosses is a second BAE branch.

In Fig 4a it is evident that there is no significant difference between the real BAE frequency (squares) calculated with and without circulating particles, and in both cases the frequency slightly drops with the increase of Ω_*. Fig 4.b, meanwhile, shows non-negligible difference in the imaginary frequencies when trapped particles are included. This effect is, however, due to the diminished Landau damping by circulating particles, and it does not imply a destabilizing role of trapped particles. On the other hand it does imply that a calculation of the threshold of the excitation of the Alfvénic ion temperature gradient driven branch [10, 26, 27], should take in consideration the trapped ions, even at high frequency. The BAE branch shown with crosses has significantly higher damping rate than the BAE mode, with imaginary frequency well below the ones shown in 4b. In Fig. 4c and d, where significant temperature gradient is given by $\eta_i = 1$, for both cases with and without trapped particles the BAE frequency initially drops with increasing Ω_*, but then it starts to grow to a certain level, due to the strong coupling to the KBM spectrum (read [10] for more details). The imaginary parts of BAE frequency (Fig 4.d) in some regions shows slightly more destabilizing effects when trapped particles are present.

Investigation of different values for the parameters shows that the BAE solution presented with crosses is much more damped then the typical BAE mode (Fig 4c.d), and it would be hardly observable in experiments or simulations. However, in some special cases (take for example $\tau = 1\,, \eta_i = 1$ and $\Omega_* > 2.5$) the two BAE branches

are so close to each other that they become degenerate and the BAE mode frequency starts to deviate from the solution predicted by the well circulating particle response [10]. Since these effects are typically small, we can conclude that generally there's no significant effect of the trapped particle presence on the real BAE frequency. Meanwhile some of the stability properties are modified, and we expect more significant changes with a proper treatment for barely trapped particles, especially for modes driven by a strong thermal ion gradient.

4. Low frequency regime and gap modes

The importance of trapped particle dynamics for low frequency fluctuations was pointed out in Ref. [1, 2], by taking the $|\omega| \ll \omega_{Bi}$ limit of Eq. (14) yielding:

$$\Lambda^2/I_\Phi \simeq \frac{\omega^2}{\omega_A^2}\left(1-\frac{\omega_{*pi}}{\omega}\right)\left(1+\frac{15}{16}\sqrt{2}q^2\epsilon^{-1/2}+0.5q^2\right) \quad , \tag{22}$$

with $I_\Phi \approx 1$. The $(15/16)\sqrt{2}q^2\epsilon^{-1/2}$ factor in this equation comes from both trapped particles response, accounting for $(3/4)\sqrt{2}q^2\epsilon^{-1/2}$, and from circulating particle corrections near the trapped to passing boundary, accounting for $(3/16)\sqrt{2}q^2\epsilon^{-1/2}$. Meanwhile, the $0.5q^2$ is the well circulating particles contribution [10]. Trapped particle contribution is dominant at low frequency and is $\mathrm{O}(\epsilon^{-1/2}) \gg 1$ larger than that of well circulating particles.

Equation 22 can be compared with the inertia enhancement [10, 46] given by the generalized form of Λ for $|\omega| \ll \omega_{Bi} \approx (r/R_0)^{1/2}\omega_{Ti}$:

$$\Lambda^2 = \left[\frac{\omega^2}{\omega_A^2}\left(1-\frac{\omega_{*pi}}{\omega}\right)+\Delta I\right] \quad , \tag{23}$$

with

$$\Delta I = q^2\frac{\omega^2}{\omega_A^2}\left(1-\frac{\omega_{*pi}}{\omega}\right)\left(\frac{R_0}{r}\right)^{1/2} f\left(\frac{r}{R_0}\right) \quad , \tag{24}$$

where $f(r/R_0) = 1.6 + 0.5(r/R_0)^{1/2}$, when terms up to order $(r/R_0)^{1/2}$ are kept [46]. The result is identical to the low frequency MHD result by Graves and Hastie [50]:

$$\Lambda^2 = \frac{\omega^2}{\omega_A^2}\left(1-\frac{\omega_{*pi}}{\omega}\right)\left(1+1.6q^2\epsilon^{-1/2}+0.5q^2\right) \quad . \tag{25}$$

Note that the structure of Eq. (23) is the same as that involved in the ZF polarizability [51, 52], as expected. The approximate treatment of the particles as deeply trapped/well circulating causes the difference between the factors 1.6 and $(15/16)\sqrt{2} \approx 1.3$ in Eqs. (22) and (25). Taking into account the exact bounce/transit motion of particles produces elliptic integrals in the velocity space and gives the same result as Ref. [50], while Eq. 22 can be directly obtained from the exact expression assuming small argument expansion for elliptic integrals (see [1] for details and [53] for a recent discussion of particle motions in general tokamak equilibria). The term I_Φ in Eq. (22) acts as additional inertia enhancement related to the response of low frequency perturbations to precessional motion of electrons and ions.

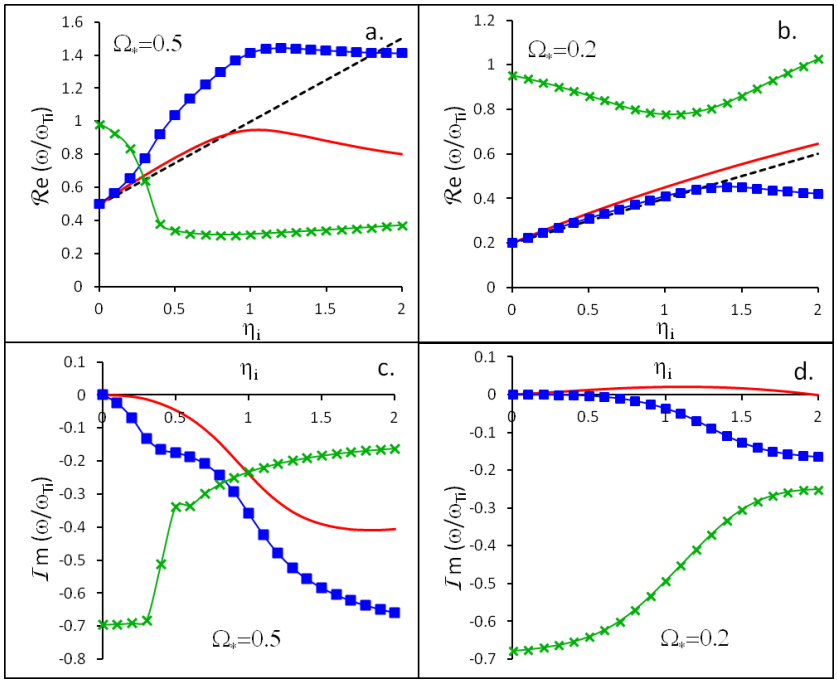

Figure 5. KBM (squares) and BAAE (crosses) accumulation point vs. $\eta_i = \omega_{*Ti}/\omega_{*ni}$ for different values of Ω_* and fixed parameters $\bar{\omega}_{Di}/\omega_{Ti} = 0.15/\sqrt{2}$, $q = 1.5$ and $\tau = 1$; Real part of the frequency (Figures a and b); Imaginary part (Figures c and d). Dashed lines ω_{*pi}/ω_{Ti}; Solid line- circulating particles only KBM accumulation point.

Trapped particles response is dominant at frequencies well below ω_{BAE} ($\overline{\omega}_{De,i} \ll \omega_{Bi} \ll \omega_{Ti} < \omega_{BAE}$). This can be demonstrated by studying trapped particle effects on kinetic balooning modes (KBMs) which, for moderate mode numbers and not so steep temperature and density profiles, have a typical frequency located inside the BAE gap. Our analysis, again, should be considered qualitative due to the model of deeply trapped particles adopted here. The real part of accumulation point frequencies of KBM and so called beta induced Alfvén acoustic Eigenmode (BAAE) are shown in Fig. 5a and b vs. $\eta_i = \omega_{*Ti}/\omega_{*ni}$ for two different values of $\Omega_* = \omega_{*ni}/\omega_{Ti}$, while the corresponding imaginary parts are shown in Fig. 5c and d. The dashed line represents ω_{*pi}/ω_{Ti}, the solid red line is KBM frequency when only circulating particles are considered, and the *blue* line with squares is KBM frequency when trapped particles are included. The results show that for $\eta_i = 0$ the KBM accumulation point is the same with and without trapped particles, but for increasing η_i the lines deviate from ω_{*pi}/ω_{Ti}; and the presence of trapped particles shifts the frequency upward for $\Omega_* = 0.5$ and downward for $\Omega_* = 0.2$ (see also Ref. [2]). These different behaviors are clearly due to the intersection or not of the two branches (green with crosses and blue with squares; *i.e.*, KBM) in complex frequency space, with Ω_* as control parameter [10].

In Fig. 5, the second branch marked with green crosses corresponds to the BAAE in the limit of small diamagnetic effects. BAAE is one of the branches of low frequency ideal MHD equations for toroidal plasmas with finite compressibility [54, 11]. It is a

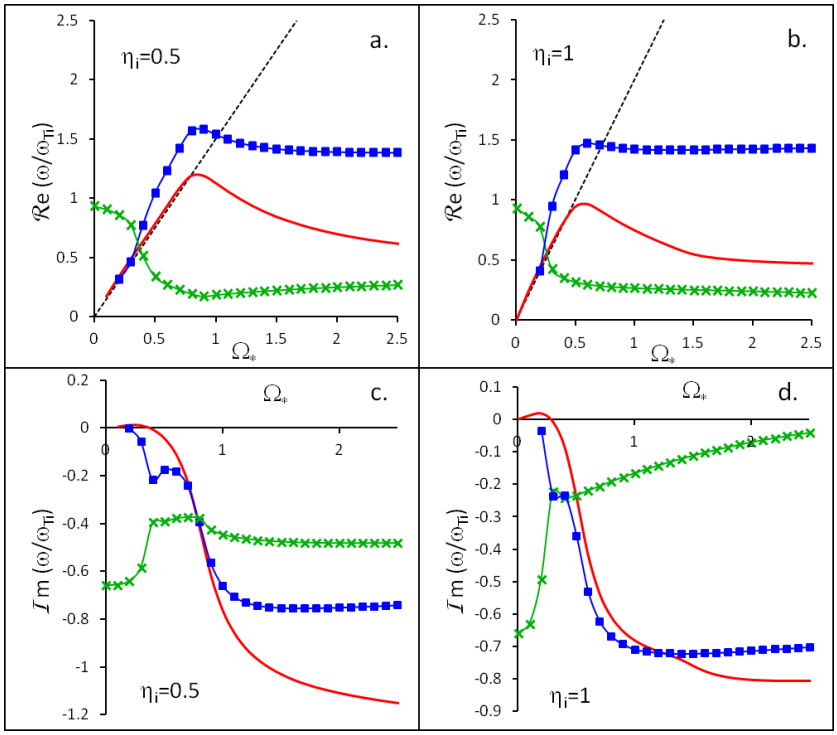

Figure 6. KBM (squares) and BAAE (crosses) vs Ω_* for fixed parameters $\bar{\omega}_{Di}/\omega_{Ti} = 0.15/\sqrt{2}$, $q = 1.5$ and $\tau = 1$; Real part of the frequency (Figures a and b); Imaginary part (Figures c and d). Dashed lines represent ω_{*pi}/ω_{Ti}. KBM with circulating particles only - solid line.

mode of mixed Alfvénic-acoustic polarization with frequency $\omega \sim \omega_{Ti}$ and at the lowest order, it can be viewed as toroidal sideband of the electrostatic drift wave [23]. Thus, it can be found in the kinetic model of low frequency Alfvén spectrum in the limit where the denominator in Eq. (9) tends to zero, or equivalently, when $\delta\Phi_s \approx \delta\Phi^{(0)}$ or even larger. Generally, in the present work we define BAAE as the solution of dispersion relations with large values for $|S| \gg \beta^{1/2}$ ($\approx$ O(1)) in Eq. (9) that, recalling $\delta\Phi^{(0)} = \delta\Psi^{(0)}$ and $\delta\Psi^{(1)} = 0$, causes a significant parallel electric field due to the high value of $\delta\Phi_s$. Figures 5a and c, show that the KBM spectrum (blue squares) is strongly coupled with the BAAE (green crosses). Meanwhile, Figures 5a through d suggest that KBM-BAAE coupling is due to diamagnetic effects, as trapped particle response, responsible for the deviation of the solid red line from the blue line with squares, is clearly not crucial. The same figures also show that when diamagnetic effects are negligible, the BAAE is heavily damped, as expected [23], but the picture may change when significant ion temperature gradient is present. These results suggest the crucial role that η_i may play in determining the necessary conditions under which BAAE, or modified DW in the more rigorous definition introduced above, can be excited by energetic particle drive.

In Fig. 6, the KBM and BAAE frequencies are given vs. Ω_* for two values of $\eta_i = 0.5$ and 1. In both cases, we find that KBM plots with (squares) and without (solid line) trapped particles are close to each other and to the ω_{*pi} line for small Ω_*,

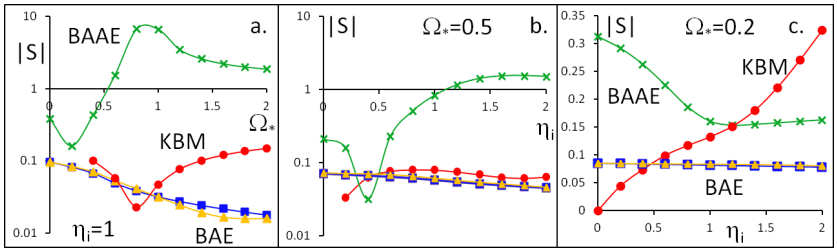

Figure 7. The value of $|S|$ for BAE (squares and triangles), KBM (circles) and BAAE (crosses) for fixed $\bar{\omega}_{Di}/\omega_{Ti} = 0.15/\sqrt{2}$, $q = 1.5$ and $\tau = 1$.

with the trapped particles shifting the frequency significantly upward as Ω_* increases. Plots with smaller values of η_i ($\eta_i < 0.25$, not shown in the figure; see Ref. [2]), show no difference between the spectra with and without trapped particles. In Fig. 6, again, we notice that the KBM spectrum is coupled with the BAAE branch; and the real frequency with trapped particles starts to deviate from the full line in the region of relatively small values of Ω_*. The imaginary parts of the frequencies (Fig 6c and d), show that trapped particles can increase or decrease the mode damping, depending on the values of Ω_* and η_i. For increasing diamagnetic effects both KBM lines with and without trapped particle reach a pick and then decrease with growing Ω_*, due to the coupling with the BAE spectrum around $\Omega_* \simeq 0.5$ located above the KBM spectrum (compare to Fig. 4b and Ref. [10]).

The values of $|S|$ are given in Fig. 7 for the modes discussed so far. In all cases, BAE (both branches) has small values for $|S| \lesssim 0.1$, while BAAE has generally large ($\approx$ O(1)) values. The simultaneous change of the $|S|$ function for BAAE and KBM suggests that the coupling between these two branches, discussed above, is also related to the parallel electric field due to $\delta\Phi_s$. In Fig. 7c, however, which corresponds to the parameters in Fig. 5b and d, the KBM value for $|S|$ becomes larger than that of BAAE when going to high η_i. For this parameter set, the real part of BAAE frequency is following Ω_*, while both modes have similar damping rate, the BAAE being slightly more damped than KBM. Thus, these branches would be experimentally identified the other way around (the BAAE as KBM and the KBM as BAAE). Although our classification of low frequency modes is just one among all possible choices, it is based on analytic continuation and mode polarization; and, in this specific case of Fig. 5b and d and Fig. 7c, is quite straightforward.

In conclusion, trapped particle response has significant impact on the properties of the low frequency modes (KBM and BAAE); and even with the approximate model of deeply trapped particles we can provide detailed descriptions of mode characteristics, as well as produce new findings concerning their mutual interaction due to finite parallel electric field and diamagnetic effects, especially in the presence of finite ion temperature gradient.

5. Conclusions and discussion

We have examined the low frequency shear Alfvén and acoustic wave spectra in toroidal geometry, taking into account wave-particle interactions with magnetically trapped and circulating particles, following the framework of the generalized fishbone-like dispersion relation. Numerical solutions for the accumulation point frequency ($\Lambda = 0$) of the shear Alfvén continuum show the possibility of co-existence of multiple solutions of the dispersion relation, *i.e.*, multiple branches of the same Beta-induced Alfvén Eigenmode. This is generally not an issue as far as identification of experimentally observed modes are concerned, since multiple modes are typically affected by strong damping. This feature is a consequence to be expected of the transcendental character of the low-frequency dispersion function accounting for wave-particle resonances with thermal plasma species. Effects of trapped particles are shown to be important for proper description of low frequency modes, such as, kinetic balooning modes and beta-induced Alfvén-acoustic eigenmodes, which proves that kinetic theory is necessary for the proper treatment of mode structures and stability conditions at frequency of the order of or lower than the thermal ion transit frequency ω_{Ti}. The mutual coupling of low frequency KBMs and BAAEs has strong effect on the real frequency and damping rate of both modes, which is of particular interest for identification of scenarios in which otherwise heavily damped BAAE modes, could be excited by energetic particles and/or thermal plasma gradients. For some plasma parameters, the two modes be strongly coupled, which means there could be a smooth transition from KBM to BAAE and vice-versa. This interplay of different low-frequency fluctuation branches has important implications on a number of kinetic stability problems as well as long time scale plasma behaviors, since realistic tokamak plasmas are characterized by complex behaviors due to the mutual interactions of SAW, MHD and Drift Wave Turbulence (DWT) [55, 56].

Acknowledgments

Useful discussions with Liu Chen, Diarmuid Curran, Philipp Lauber, Zhiyong Qiu and Xin Wang are kindly acknowledged.

Bibliography

[1] Chavdarovski I and Zonca F 2009 *Plasma Phys. Contr. Fusion* **51** 115001
[2] Chavdarovski I 2009 Kinetic theory of low frequency Alfvén waves in burning plasmas *PhD Thesis University of Tor Vergata*
[3] Heidbrink W W, Strait E J, Chu M S and Turnbull A D 1993 Phys. Rev. Lett. **71** 855
[4] Turnbull A D et al 1993 *Phys. Fluids B* **5** 2546
[5] Berk H L et al 2006 *Nucl. Fusion* **46** S888
[6] Boswell C J et al 2006 *Phys. Lett. A* **358** 154
[7] Darrow D S et al 2008 *Nucl. Fusion* **48** 084004
[8] Van Zeeland M A et al 2008 Alfvénic Instabilities and Fast Ion Transport in the DIII-D Tokamak

Proc. 22nd Int. Fusion Energy Conf. 2008 (Geneva, 2008) (Vienna: IAEA) CD-ROM file EX/6-2

[9] Nazikian R et al 2008 *Phys. Rev. Lett.* **101** 185001
[10] Zonca F, Chen L and Santoro R A 1996 *Plasma Phys. Control. Fusion* **38** 2011
[11] Gorelenkov N N, Berk H L, Fredrickson E and Sharapov S E 2007 *Phys. Lett. A* **370** 70
[12] Gorelenkov N N et al 2007 *Plasma Phys. Control. Fusion* **49** B371
[13] Gorelenkov N N et al 2008 Theory and observations of low frequency eigenmodes due to Alfvén acoustic coupling in toroidal fusion plasmas *Proc. 22nd Int. Fusion Energy Conf. 2008 (Geneva, 2008)* (Vienna: IAEA) CD-ROM file TH/5-2
[14] Gorelenkov N N 2008 50th APS-DPP Annual Meeting (Dallas, Texas) GI1.00002
[15] Smolyakov A I, Garbet X, Falchetto G and Ottaviani M 2008 *Phys. Lett. A* **372** 6750
[16] Smolyakov A I, Nguyen C and Garbet X 2008 *Plasma Phys. Control. Fusion* **50** 115008
[17] N. N. Gorelenkov, M. A. Van Zeeland, H. L. Berk, N. A. Crocker, D. Darrow, E. Fredrickson, G.-Y. Fu, W. W. Heidbrink, J. Menard and R. Nazikian 2009 *Phys. Plasmas* **16** 056107
[18] Liu Yi, Isobe Mitsutaka, Peng Xiao-Dong, Wang Hao, Ji Xiao-Quan, Chen Wei, Zhang Yi-Po, Dong Yun-Bo, Morita Shigeru, Toi Kazuo and Duan Xu-Ru 2012 *Nucl. Fusion* **52** 074008 (7pp)
[19] Connor J W and Chen L 1985 *Phys. Fluids 28* 2201
[20] Zonca F, Chen L, Botrugno A, Buratti P, Cardinali A, Cesario R, Pericoli Ridolfini V and JET EFDA contributors 2009 *Nucl. Fusion* **49** 085009
[21] Ph. Lauber, M. Brüdgam, D. Curran, V. Igochine, K. Sassenberg, S. Günter, M. Maraschek, and M. Garc´ia-Muñoz, N. Hicks and the ASDEX Upgrade Team *Plasma Phys. Control. Fusion* **51**, 124009 (2009)
[22] Lauber Ph et al 2009 Damping and Drive of Alfvén Eigenmodes at ASDEX Upgrade *36th EPS Conference on Plasma Phys. (Sofia, 29 June - 3 July 2009)* I-5.077
[23] Zonca F, Biancalani A, Chavdarovski I, Chen L, Di Troia C and Wang X 2010 *Journal of Physics: Conference Series* **260** 012022
[24] Curran D, Lauber Ph, Mc Carthy P J, da Graça S, Igochine V and the ASDEX Upgrade Team *2012 Plasma Phys. Control. Fusion* **54** *055001*
[25] Nguyen C, Garbet X and Smolyakov A I 2008 *Phys. Plasmas* **15** 112502
[26] Zonca F, Chen L, Santoro R A and Dong J Q 1998 *Plasma Phys. Control. Fusion* **40** 2009
[27] Zonca F, Chen L, Dong J Q and Santoro R A 1999 *Phys. Plasmas* **6** 1917
[28] Mikhailovskii A B and Sharapov S E 1999 *Plasma Phys. Rep.* **25** 838
[29] Zonca F and Chen L 2008 *Europhys. Lett.* **83** 35001
[30] Sugama H and Watanabe T-H 2006 *Phys. Plasmas* **13** 012501
[31] Gao Z, Itoh K, Sanuki H and Dong J Q 2006 *Phys. Plasmas* **13** 100702
[32] Qiu Z Y, Chen L and Zonca F 2009 *Plasma Phys. Control. Fusion* **51** 012001
[33] Chen L, White R B and Rosenbluth M N 1984 *Phys. Rev. Lett.* **52** 1122
[34] Tsai S T and Chen L 1993 *Phys. Fluids* **B 5** 3284
[35] Chen L 1994 *Phys. Plasmas* **1** 1519
[36] Hu B, Betti R and Manickam J 2006 *Phys. Plasmas* **13** 112505
[37] Annibaldi S V, Zonca F and Buratti P 2007 *Plasma Phys. Control. Fusion* **49** 475
[38] Zonca F and Chen L 2006 *Plasma Phys. Controlled Fusion* **48** 537
[39] Connor J W, Hastie R J and Taylor J B 1978 *Phys. Rev. Lett.* **40** 396
[40] Antonsen T M and Lane B 1980 *Phys. Fluids* **23** 1205
[41] Chen L and Hasegawa A 1991 *Journal of Geographical Research* **96(A2)** 1503
[42] H. Hasegawa and L. Chen, Phys. Rev. Lett. **35**, 370 (1975)
[43] H. Hasegawa and L. Chen, Phys. Fluids **19**, 1924 (1976)
[44] Chen L and Zonca F 2007 *Nucl. Fusion* **47** S727
[45] Garbet X et al 2006 Theory of Fusion Plasmas *AIP Conference Proceedings* **871** 342
[46] Zonca F et al 2007 *Nucl. Fusion* **47** 1588
[47] Zonca F 2008 *Int. J. Mod. Phys. A* **23** 1165

[48] Wang X, Zonca F and Chen L 2010 *Plasma Phys. Control. Fusion* **52** 115005
[49] Tang W M, Connor J W and Hastie R J 1980 *Nucl. Fusion* **20** 1439
[50] Graves J P, Hastie R J and Hopcraft K I 2000 *Plasma Phys. Control. Fusion* **42** 1049
[51] Rosenbluth M N and Hinton F L 1998 *Phys. Rev. Lett.* **80** 724
[52] Hinton F L and Rosenbluth M N 1999 *Plasma Phys. Control. Fusion* **41** A653
[53] Graves J P 2013 *Plasma Phys. Control. Fusion* **55** 074009
[54] Cheng C Z and Chance M S 1986 *Phys. Fluids* **29** 3695
[55] Zonca F and Chen L 2008 "Structures of the low frequency Alfvén continuous spectrum and their consequences on MHD and micro-turbulence" Theory of Fusion Plasmas *AIP Conference Proceedings* **1069** 355
[56] Zonca F and Chen L 2008 "Nonlinear Dynamics and Complex Behaviors in Magnetized Plasmas of Fusion Interest" Frontiers in Modern Plasma Physics *AIP Conference Proceedings* **1061** 34